5-10-2013

Time-resolved ultrafast electron (e,2e) momentum spectroscopy

Hua-Chieh Shao
University of Nebraska-Lincoln, s-hshao1@unl.edu

Anthony F. Starace
University of Nebraska-Lincoln, astarace1@unl.edu

PHYSICAL REVIEW A **87**, 050701(R) (2013)

Time-resolved ultrafast electron $(e,2e)$ momentum spectroscopy

Hua-Chieh Shao and Anthony F. Starace
Department of Physics and Astronomy, The University of Nebraska, Lincoln, Nebraska 68588-0299, USA
(Received 6 March 2013; published 10 May 2013)

The $(e,2e)$ process is analyzed for the case of an ultrafast electron pulse incident upon a target prepared in a time-varying, coherent superposition of states. Conditions under which time-resolved target momentum densities can be obtained from experimental measurements are discussed. Results for coherent electronic motions in both the H atom and the H_2^+ molecule are used to illustrate the capability of an ultrafast electron pulse to image time-dependent target electron dynamics.

DOI: 10.1103/PhysRevA.87.050701 PACS number(s): 03.65.Nk, 34.80.Dp, 34.80.Gs

The last decade has seen growing interest in attosecond science [1,2], one of whose goals is to image time-resolved electron dynamics. Owing to advances in strong-field physics, unprecedented time resolutions have been attained, and various paradigms have been demonstrated for investigating ultrafast dynamics in atoms, molecules, and solids. In self-probing approaches [3], for example, in which residual ions are probed by one of their own laser-driven electrons, high harmonic generation spectra have been used for tomographic reconstruction of molecular orbitals of N_2 [4] and CO_2 [5] and laser-induced electron diffraction spectra have been used to probe ultrafast changes of the bond lengths of O_2 and N_2 during the ionization process [6]. These successful advances that use electrons to probe molecular structures are nevertheless limited by the parameters of the driving laser fields. Alternatively, ultrashort electron pulses have also been used to probe the ultrafast dynamics of molecules and solids [7–10]. Moreover, ways of generating ultrashort electron pulses with attosecond durations have been proposed, either by pulse compression [11–14] or by dispersion compensation [15]. Attosecond electron pulse scattering experiments have been proposed and simulated as a means to image target electron dynamics [16–18].

Stationary states of atoms and molecules have been imaged using $(e,2e)$ momentum spectroscopy [19–22]. In kinematically complete measurements, the ejected electrons can be analyzed to select ionized valence electrons, which are the participants in chemical reactions [21]. Since symmetry properties of spatial wave functions are preserved in momentum space [20], these symmetries can be determined from measured momentum space densities. Thus, ultrafast electron momentum spectroscopy is potentially an excellent tool for investigating time-dependent electron dynamics.

We propose here to use attosecond electron pulses as probes of electron dynamics in atoms and molecules (initiated, e.g., by a pump laser) by means of $(e,2e)$ measurements, in order to obtain time-resolved momentum densities $\rho(\mathbf{q},t)$ of target electrons. We describe the $(e,2e)$ process for an ultrafast electron pulse incident at time $t = 0$ on a time-varying coherent target state that we assume is produced at time $t = -t_d$, where t_d is the delay time between production of the target state and the collision. The symmetric-noncoplanar setup [20] is chosen since measurements are then directly related to $\rho(q_z,t_d)$, which is measured by varying the azimuth angle ϕ of the detectors (see Fig. 1). We employ atomic units.

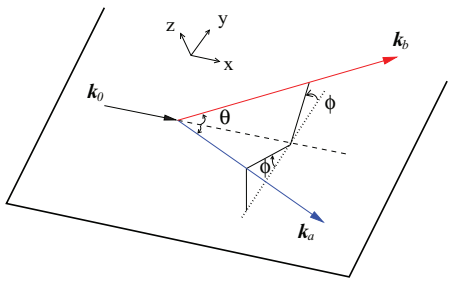

FIG. 1. (Color online) The symmetric-noncoplanar setup of a pump-probe experiment to image the time-resolved momentum density of target electrons. The momenta of the incident, scattered, and ejected electrons are denoted by $\boldsymbol{k}_0$, $\boldsymbol{k}_a$, and $\boldsymbol{k}_b$, respectively.

For an electron with momentum $\boldsymbol{k}_0$ incident on a target atom or molecule A having momentum $\boldsymbol{k}_1$, the electron impact ionization [or $(e,2e)$] process we consider is

$$e^-(\boldsymbol{k}_0) + \mathrm{A}(\boldsymbol{k}_1,n) \to e^-(\boldsymbol{k}_a) + e^-(\boldsymbol{k}_b) + \mathrm{A}^+(\boldsymbol{k}_c,m),$$

where $\boldsymbol{k}_a$ and $\boldsymbol{k}_b$ are the momenta of the scattered and ionized electrons, and $\boldsymbol{k}_c$ is that of the residual ion. The target has some time-dependent internal structure to be probed. The eigenstates of the target and the ion are specified, respectively, by the sets of quantum numbers n and m. To describe scattering of an electron from a coherent electronic state, an appropriate collision theory must be developed. Robicheaux has studied inelastic scattering of coherent matter beams from a target [23]. Among his findings is that the transition probability to a different bound state of the target depends on the amplitudes for the initial states, not their populations. We generalize Robicheaux's analysis to describe electron impact ionization or $(e,2e)$ processes in the case of a coherent incident electron beam and target state.

Consider a coherent wave packet describing both incident electron and time-dependent target state at $t = 0$,

$$\psi_{\mathrm{coh}}^{(+)} = \int d\boldsymbol{k}_0\, d\boldsymbol{k}_1\, a_0(\boldsymbol{k}_0) a_1(\boldsymbol{k}_1) \sum_n C_n\, \psi_i^{(+)}, \qquad (1)$$

where a_0 (a_1) is the momentum distribution of the incident electron (target), C_n is the amplitude of the target internal state n, and $\psi_i^{(+)}$ is the eigenstate of the full Hamiltonian, for entrance channel $i \equiv \{\boldsymbol{k}_0,\boldsymbol{k}_1,n\}$ with energy ε_i, satisfying outgoing wave boundary conditions. Unlike the conventional

treatment [19,20], in which a_1 is omitted, $\psi_{\rm coh}^{(+)}$ describes both the projectile and the target by wave packets. This is necessary to observe the time-dependent internal structure of the target. The transition probability density $|\mathscr{A}_f|^2$ to some final state ψ_f is [24]

$$|\mathscr{A}_f|^2 = \sum_{n'n} C_{n'}^* C_n \int d\boldsymbol{k}_0' \, d\boldsymbol{k}_1' \, d\boldsymbol{k}_0 \, d\boldsymbol{k}_1 \, a_0^*(\boldsymbol{k}_0') a_0(\boldsymbol{k}_0) \times a_1^*(\boldsymbol{k}_1') a_1(\boldsymbol{k}_1) (2\pi)^2 \delta(\varepsilon_f - \varepsilon_{i'}) \delta(\varepsilon_f - \varepsilon_i) \times \delta(\mathcal{P}_f - \mathcal{P}_{i'}) \delta(\mathcal{P}_f - \mathcal{P}_i) \, T_{fi'}^* T_{fi}, \quad (2)$$

where $i' \equiv \{\boldsymbol{k}_0', \boldsymbol{k}_1', n'\}$, $\mathcal{P}_i \equiv \boldsymbol{k}_0 + \boldsymbol{k}_1$ and $\mathcal{P}_{i'} \equiv \boldsymbol{k}_0' + \boldsymbol{k}_1'$ are the total linear momenta of the initial eigenstates i and i', $\mathcal{P}_f \equiv \boldsymbol{k}_a + \boldsymbol{k}_b + \boldsymbol{k}_c$ and ε_f are the momentum and energy of the final state $f \equiv \{\boldsymbol{k}_a, \boldsymbol{k}_b, \boldsymbol{k}_c, m\}$, and T_{fi} is the transition matrix element of the Coulomb interaction between incident and target electrons. One sees that $|\mathscr{A}_f|^2$ has contributions from different initial states i, i' and that each of them satisfies momentum and energy conservation. The transition probability $\mathscr{P}$ for a measurement is the integral of $|\mathscr{A}_f|^2$ over the parameters of the detectors,

$$\mathscr{P} = \sum_m \int d\boldsymbol{k}_a \, d\boldsymbol{k}_b \, d\boldsymbol{k}_c |\mathscr{A}_f|^2. \quad (3)$$

In principle, interference of different momentum components may affect the ability to accurately image the target electron momentum density $\rho(\mathbf{q},t)$. In practice, for a high incident electron energy and a large target mass m_1, T_{fi} is insensitive to variations of the electron and target momenta within the wave-packet amplitudes $a_0(\boldsymbol{k}_0)$ and $a_1(\boldsymbol{k}_1)$. In fact, $\mathscr{P}$ can be simplified by approximating T_{fi} by its value at the central momenta $m_0\boldsymbol{v}_0$ ($m_0 = 1$ in a.u.) and $m_1\boldsymbol{v}_1$ of the incident electron and the target. One then has to carry out integrations over the energy and momentum delta functions. The integrations over $E_b \equiv k_b^2/2$, $\boldsymbol{k}_c$, and $\boldsymbol{k}_1'$ are trivial. The integration over $\boldsymbol{k}_0'$ is separated into those for its components $\boldsymbol{k}_{0\perp}'$ and $k_{0\parallel}'$ perpendicular and parallel to $\boldsymbol{v}_0$ and the integration over $k_{0\parallel}'$ is done as in Sec. IIB of Ref. [23]. If the width of a_1 is assumed to be much larger than that of a_0 (along both the $k_{1\parallel}$ and $\boldsymbol{k}_{1\perp}$ directions), the $\boldsymbol{k}_1$ integral can be done straightforwardly [24]. The result of these integrations is the triple differential probability (TDP) $d^3\mathscr{P}/dE_a d\hat{\boldsymbol{k}}_a \, d\hat{\boldsymbol{k}}_b$ for electron impact ionization from a coherent state:

$$\frac{d^3\mathscr{P}}{dE_a \, d\hat{\boldsymbol{k}}_a \, d\hat{\boldsymbol{k}}_b} \simeq \sum_{mn'n} \mathcal{B}_{n'n} C_{n'}^* C_n \frac{|\boldsymbol{k}_a||\boldsymbol{k}_b|}{|\boldsymbol{v}_0 - \boldsymbol{v}_1|} T_{fi'}^* T_{fi}, \quad (4)$$

where

$$\mathcal{B}_{n'n} = (2\pi)^2 \int d\boldsymbol{k}_{0\perp}' \, d\boldsymbol{k}_0 \, a_0^*(k_{0\parallel} - \Delta k, \boldsymbol{k}_{0\perp}') \, a_0(\boldsymbol{k}_0). \quad (5)$$

In Eq. (5), $\Delta k \equiv (\omega_{n'} - \omega_n)/|\boldsymbol{v}_0|$, where ω_n is the energy eigenvalue of the target state n. Equations (4) and (5) generalize and combine Robicheaux's treatment of scattering from a coherent state [cf. Eq. (12) in [23]] and the usual $(e,2e)$ scattering formulas [cf. Eq. (3.1) in [20]]. Note that information on the internal structure of the target is embedded in T_{fi} and the amplitudes C_n.

For scattering of ultrafast electron pulses ($\gtrsim 1$ keV) with kinematics near the Bethe ridge [25] ($|\boldsymbol{v}_0 - \boldsymbol{k}_a| \approx |\boldsymbol{k}_b|$), the plane-wave impulse approximation (PWIA) is adequate to evaluate T_{fi} for small target electron momentum $\boldsymbol{q}$ ($|\boldsymbol{q}| \lesssim 1.5$ a.u.) [19–22]. In the PWIA, the incident electron interacts with only one target electron at a time, and interactions with other electrons and nuclei are neglected, so the many-particle T_{fi} is replaced by a two-particle one. For many-electron targets, if the target and ion orbital wave functions are calculated in the frozen-core Hartree-Fock approximation, then T_{fi} is proportional to the momentum space wave function ϕ_n of the orbital from which the target electron is ionized [19–22]. Specifically, the TDP can be written as

$$\frac{d^3\mathscr{P}}{dE_a \, d\hat{\boldsymbol{k}}_a \, d\hat{\boldsymbol{k}}_b} \simeq (2\pi)^{-4} \sum_{n'n} \mathcal{B}_{n'n} C_{n'}^* C_n \frac{|\boldsymbol{k}_a||\boldsymbol{k}_b|}{|\boldsymbol{v}_0 - \boldsymbol{v}_1|} \frac{4}{s^4} \times \phi_{n'}^*(\boldsymbol{q}) \phi_n(\boldsymbol{q}), \quad (6)$$

where ϕ_n is the Fourier transform of the target-ion overlap, $\boldsymbol{s} \equiv \boldsymbol{v}_0 - \boldsymbol{k}_a$ is the momentum transfer of the scattered electron, and $\boldsymbol{q} = \boldsymbol{k}_a + \boldsymbol{k}_b - \boldsymbol{v}_0$ is the target electron momentum at the time of the collision. Owing to velocity mismatch of laser pump and electron probe pulses (assuming the target coherent state is produced by a laser pulse), $\mathscr{P}$ depends in general on the position of the target (through the phase of the coefficients C_n). However, a technique exists for overcoming the velocity mismatch [9,26]. Thus, we ignore this effect and set $C_n = c_n e^{-i\omega_n t_d}$, where c_n is the amplitude of the target state n at the time it is produced (i.e., at $t_d = 0$). Note that if $\mathcal{B}_{n'n}$ in Eq. (6) depends only weakly on n and n' (through Δk), then the TDP is proportional to $\rho(q_z,t_d)$ of the coherent state, i.e., $d^3\mathscr{P}/dE_a \, d\hat{\boldsymbol{k}}_a \, d\hat{\boldsymbol{k}}_b \propto |\sum c_n e^{-i\omega_n t_d} \phi_n(q_z)|^2 \equiv \rho(q_z,t_d)$. In general, to image $\rho(q_z,t)$ of the coherent state, a_0 must have a coherent width larger than Δk.

To illustrate the capability of ultrafast $(e,2e)$ momentum spectroscopy, we consider coherent electronic states of the prototypical H atom and H_2^+ molecular ion. For the H atom, we consider a coherent superposition of the $3p$ and $4p$ states, produced as detailed in Ref. [18]. Briefly, the H atom is excited from the $1s$ state by a laser pulse, linearly polarized along the z axis, whose bandwidth and photon energy are chosen such that the $3p$ and $4p$ populations are equal; the beat period $\mathsf{T} = 2\pi/(\omega_{4p} - \omega_{3p})$ of this coherent state is 6.25 fs. The momentum densities $\rho(q_z,t)$ along the polarization axis for $t = 0, 1/4, 1/2$ T are shown in Fig. 2(a). Their symmetric distribution implies symmetric motion of the charge density; the valley at the origin originates from the nonzero orbital angular momentum of the state. As time increases, the width of the momentum distribution contracts, which implies that the width of the corresponding charge distribution expands. Note that for all times, the momenta are $\lesssim 0.3$ a.u. In order to image $\rho(q_z,t)$ of a state having such small momenta, the parameters for the momentum distribution of the incident electron and for the angular resolution of the measurement must be chosen carefully [27].

In order to show that the TDP in Eq. (6) is, for appropriate experimental parameters, indeed proportional to $\rho(q_z,t)$ of the coherent state, we calculate $\mathscr{P}$ in the PWIA using Eqs. (2) and (3), i.e., we do not approximate T_{fi} using the central

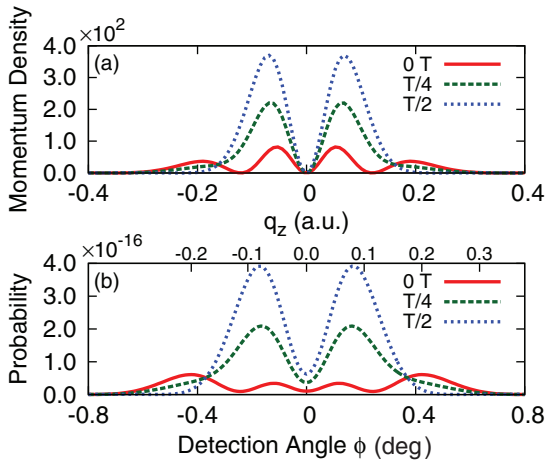

FIG. 2. (Color online) Comparison of (a) the momentum density $\rho(q_z,t)$ of a coherent superposition of the $3p$ and $4p$ states of H (beat period $\mathsf{T} = 6.25$ fs) with (b) the transition probability $\mathscr{P}$ [cf. Eqs. (3) and (2)] for $(e,2e)$ scattering of a 10 keV, 100 as electron pulse from that state at delay times $t_d = 0$, 1/4, and 1/2 T.

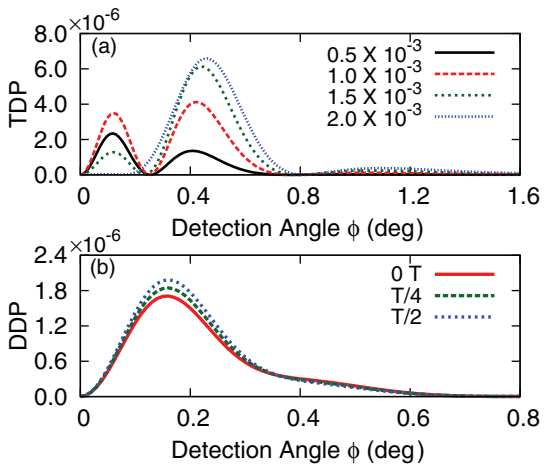

FIG. 3. (Color online) Effects of (a) transverse and (b) longitudinal interference. (a) The TDPs for four different beam angular spreads $\Delta\theta_0$ at delay time $t_d = 0$. (b) The DDP of a 5-fs-duration pulse at three different delay times t_d. Owing to symmetry about $\phi = 0$, only $\phi \geqslant 0$ results are shown. See text for details.

momentum of the incident electron wave packet, as was done to derive Eq. (4). We choose the energy of the electron pulse to be 10 keV (one of the cases considered in Ref. [12]) and its FWHM duration to be 100 as. The kinetic energy of the target is assumed to be 25 meV. The amplitude a_0 is modeled by a Gaussian distribution with longitudinal and transverse widths set by the incident electron pulse duration and angular spread $\Delta\theta_0$, where $\cos\theta_0 = \hat{\boldsymbol{k}}_0 \cdot \hat{\boldsymbol{x}}$. We assume $\Delta\theta_0 = 10^{-3}$ rad. The scattering angle is $\theta = 45^\circ$, and the detection window $\theta \times \phi$ is $0.2^\circ \times 0.2^\circ$ [in order to resolve accurately $\rho(q_z,t)$]. The detector energy resolution is taken as 3 eV centered at half the average final kinetic energy ($\approx$5 keV). For the symmetric-noncoplanar setup, q_z and the detection angle ϕ are related by [20]

$$q_z = \sqrt{2E_0}\,\sin\frac{\phi}{2}, \tag{7}$$

where E_0 is the kinetic energy of the incident electron, and $E_0 \gg \omega_n$ is assumed. The calculated $\mathscr{P}$ for three delay times t_d are shown in Fig. 2(b).

Comparing $\mathscr{P}$ in Fig. 2(b) with $\rho(q_z,t)$ in Fig. 2(a) shows quite good agreement, with the following differences. First, the widths of the peaks in $\mathscr{P}$ are wider due mainly to the finite detection window. Second, $\mathscr{P}$ preserves both the symmetry of $\rho(q_z,t)$ and the valley about $q_z = 0$ typical of states with nonzero angular momentum (although $\mathscr{P}$ is small but nonzero at the origin). Third, the stationary point in the momentum density around $q_z \approx \pm 0.16$ a.u. is reproduced in $\mathscr{P}$ at $\phi \approx \pm 0.38^\circ$. This is due to the innermost node of the $4p$ momentum wave function $\phi_{4p}(q_z)$. Finally, the ratio ($<$1) of the inner and outer peak maxima in the $\mathscr{P}$ curve for $t_d = 0$ T is opposite to the ratio ($>$1) of those peaks in the corresponding momentum density curve.

To isolate the origin of the latter discrepancy in the peak ratios of the $t_d = 0$ T curves in Fig. 2, the TDPs are calculated for different $\Delta\theta_0$ at $t_d = 0$ T, as shown in Fig. 3(a). To obtain these results the $\boldsymbol{k}_1$ integral in Eq. (2) is done numerically, i.e., we do not assume that the width of a_1 is much larger than that of a_0 as in Ref. [24]. We assume a Gaussian distribution for a_1 with a width of 0.6 a.u. For $\Delta\theta_0 = 0.5 \times 10^{-3}$ rad. the ratio of the inner and outer peak maxima is $>$1, just as in the momentum density in Fig. 2(a). For larger $\Delta\theta_0$, this peak ratio declines and for $\Delta\theta_0 = 2.0 \times 10^{-3}$ rad. the inner peak maximum is not visible. As $\Delta\theta_0$ increases, the incident angle of the electron pulse becomes less well defined, and hence scattering amplitudes with different incident angles interfere. Whereas in Fig. 3(a) we show effects of transverse interference, in Fig. 3(b) we show effects of longitudinal interference by exhibiting the dependence on delay time t_d of the double differential probabilities (DDPs) $d^2\mathscr{P}/d\hat{\boldsymbol{k}}_a\,d\hat{\boldsymbol{k}}_b$ [cf. Eq. (3)] for an incident electron pulse of 5 fs duration and a detector energy resolution of 3 eV. Clearly the momentum width is too narrow, so that the pulse has insufficient time resolution. Hence, the DDP approximates the sum of the momentum densities of the $3p$ and $4p$ orbitals, with little time dependence.

For $H_2{}^+$, we assume an equal superposition of $\sigma_g 1s$ and $\sigma_u 1s$ states for large bond length R [18,28,29]. At equilibrium the energy between adjacent electronic levels is usually several eVs for the lowest-lying states. However, at large bond length the electronic levels are closer, and, accordingly, coherent electron motion occurs over a larger time scale. Contrary to the case treated above for the H atom, the states $\sigma_g 1s$ and $\sigma_u 1s$ have opposite parity, and the electron charge density oscillates between the two nuclei, i.e., there is charge transfer from one site to the other. For $R = 6$ a.u., the beat period is $\mathsf{T} = 7.1$ fs. The Born-Oppenheimer approximation is assumed valid, and the molecular orbitals are constructed using a linear combination of atomic orbitals. The energy levels of the lowest two states are well separated from other excited states, implying negligible contributions of excited states of the H atom to these molecular orbitals. Thus, only the $1s$ orbital of the H atom is employed. In addition, nuclear motion is assumed to be negligible.

The electronic momentum and charge densities along the molecular axis of $H_2{}^+$ as a function of time t are shown

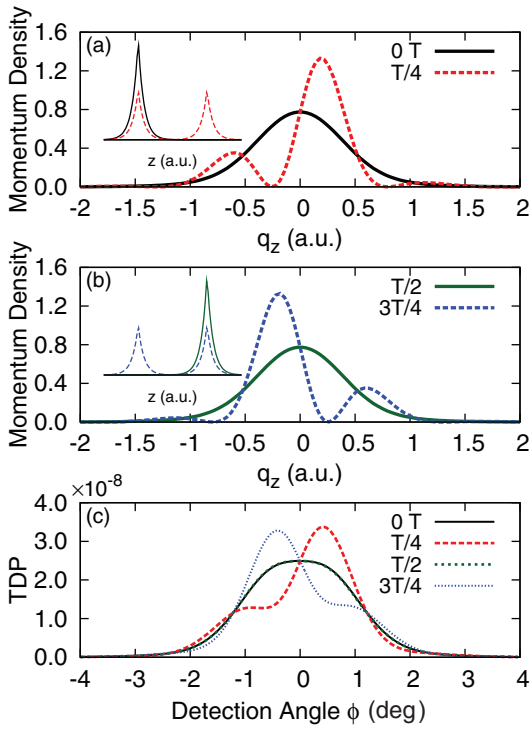

FIG. 4. (Color online) Momentum and charge (inset) densities along the molecular axis of a coherent superposition of H_2^+ $\sigma_g 1s$ and $\sigma_u 1s$ states (beat period $\mathsf{T} = 7.1$ fs) for (a) $t = 0$, $\mathsf{T}/4$ and (b) $t = \mathsf{T}/2$, $3\mathsf{T}/4$. (c) The TDP for $(e,2e)$ scattering of a 10 keV, 100 as electron pulse from that state for four values of the delay time t_d (cf. Fig. 1 and text for details).

in Figs. 4(a) and 4(b). At $t = 0\,\mathsf{T}$ the electron is localized about the left nucleus and its momentum density is similar to that of the $1s$ orbital of the H atom. As the electron moves toward the other nucleus, its momentum density shifts toward positive momenta. The TDPs calculated using Eq. (2) (in which the $\boldsymbol{k}_1$ integral is carried out as described above for H) are shown in Fig. 4(c) for different delay times t_d. The bond length R is assumed to have a Gaussian distribution with FWHM of 0.3 a.u. The molecular axis of H_2^+ is assumed to be oriented approximately perpendicularly to the incident electron pulse with an angular distribution ($\propto \cos^6\theta_{\rm mol} + \alpha\,\cos^7\theta_{\rm mol}$) chosen such that $\langle\cos^2\theta_{\rm mol}\rangle = 0.78$, which is experimentally achievable [30], and α selected such that $\langle\cos\theta_{\rm mol}\rangle = 0.39$ so that the molecule is oriented. Comparing the TDPs in Fig. 4(c) with the momentum densities $\rho(q_z,t)$ in Figs. 4(a) and 4(b) we find qualitative agreement; in particular, the left-right charge transfer motion is faithfully reproduced. Quantitatively, however, the TDPs are strongly affected by the R and $\theta_{\rm mol}$ distributions, especially the angular distribution. Precise orientation of a target molecule is essential to faithfully observe its electronic motion (because essential interference of opposite parity amplitudes is lost by averaging over a symmetric angular distribution).

In conclusion, we have demonstrated both analytically and numerically that attosecond electron pulse $(e,2e)$ processes are capable of directly imaging time-dependent momentum space densities $\rho(\boldsymbol{q},t)$ of coherent states of H and H_2^+. (This contrasts with the attosecond electron elastic scattering process considered in [18], which requires solving the inverse scattering problem to obtain time-dependent target information.) Such imaging depends crucially on the off-diagonal elements $a_0^*(\boldsymbol{k}_0')a_0(\boldsymbol{k}_0)$ of the incident electron density matrix, whose coherence is essential for imaging $\rho(\boldsymbol{q},t)$. Our simulations are based on Eqs. (2) and (3), which do not assume the factorization of T_{fi} [cf. Eqs. (4) and (5)] that lead to proportionality of the TDP and the target $\rho(q_z,t)$, where the z axis is determined by the experimental arrangement. Assuming proposals for attosecond electron pulses are realized [11–15], ultrafast $(e,2e)$ electron momentum spectroscopy can, in principle, provide the means for time-resolved measurements of electron dynamics in atoms and molecules.

We gratefully acknowledge discussions with Lars Madsen and Francis Robicheaux. This work was supported in part by NSF Grant No. PHYS-1208059.

[1] F. Krausz and M. Ivanov, Rev. Mod. Phys. **81**, 163 (2009).
[2] P. Salières, A. Maquet, S. Haessler, J. Caillat, and R. Taïeb, Rep. Prog. Phys. **75**, 062401 (2012).
[3] S. Haessler, J. Caillat, and P. Salières, J. Phys. B **44**, 203001 (2011).
[4] S. Haessler, J. Caillat, W. Boutu, C. Giovanetti-Teixeira, T. Ruchon, T. Auguste, Z. Diveki, P. Breger, A. Maquet, B. Carré, R. Taïeb, and P. Salières, Nat. Phys. **6**, 200 (2010).
[5] C. Vozzi, M. Negro, F. Calegari, G. Sansone, M. Nisoli, S. De Silvestri, and S. Stagira, Nat. Phys. **7**, 822 (2011).
[6] C. I. Blaga, J. Xu, A. D. DiChiara, E. Sistrunk, K. Zhang, P. Agostini, T. A. Miller, L. F. DiMauro, and C. D. Lin, Nature (London) **483**, 194 (2012).
[7] D. Shorokhov and A. H. Zewail, Phys. Chem. Chem. Phys. **10**, 2879 (2008); see also references therein.
[8] A. H. Zewail, Science **328**, 187 (2010).
[9] G. Sciaini and R. J. D. Miller, Rep. Prog. Phys. **74**, 096101 (2011).
[10] C. J. Hensley, J. Yang, and M. Centurion, Phys. Rev. Lett. **109**, 133202 (2012).
[11] E. Fill, L. Veisz, A. Apolonski, and F. Krausz, New J. Phys. **8**, 272 (2006).
[12] P. Baum and A. H. Zewail, Proc. Natl. Acad. Sci. USA **104**, 18409 (2007).
[13] S. A. Hilbert, C. Uiterwaal, B. Barwick, H. Batelaan, and A. H. Zewail, Proc. Natl. Acad. Sci. USA **106**, 10558 (2009).
[14] A. Gliserin, A. Apolonski, F. Krausz, and P. Baum, New J. Phys. **14**, 073055 (2012).
[15] P. Hansen, C. Baumgarten, H. Batelaan, and M. Centurion, Appl. Phys. Lett. **101**, 083501 (2012).
[16] P. Baum and A. H. Zewail, Chem. Phys. **366**, 2 (2009).
[17] P. Baum, J. Manz, and A. Schild, Sci. China Phys. Mech. Astron. **53**, 987 (2010).
[18] H.-C. Shao and A. F. Starace, Phys. Rev. Lett. **105**, 263201 (2010).
[19] I. E. McCarthy and E. Weigold, Rep. Prog. Phys. **54**, 789 (1991).

[20] M. A. Coplan, J. H. Moore, and J. P. Doering, Rev. Mod. Phys. **66**, 985 (1994).
[21] C. E. Brion, G. Cooper, Y. Zheng, I. V. Litvinyuk, and I. E. McCarthy, Chem. Phys. **270**, 13 (2001).
[22] M. Takahashi, Bull. Chem. Soc. Jpn. **82**, 751 (2009).
[23] F. Robicheaux, Phys. Rev. A **62**, 062706 (2000); see also references therein.
[24] M. L. Goldberger and K. M. Watson, *Collision Theory* (Wiley, New York, 1964).
[25] M. Inokuti, Rev. Mod. Phys. **43**, 297 (1971).
[26] P. Baum and A. H. Zewail, Proc. Natl. Acad. Sci. USA **103**, 16105 (2006).
[27] P. Duffy, M. E. Casida, C. E. Brion, and D. P. Chong, Chem. Phys. **159**, 347 (1992).
[28] G. L. Yudin, S. Chelkowski, J. Itatani, A. D. Bandrauk, and P. B. Corkum, Phys. Rev. A **72**, 051401(R) (2005).
[29] A. D. Bandrauk, S. Chelkowski, P. B. Corkum, J. Manz, and G. L. Yudin, J. Phys. B **42**, 134001 (2009).
[30] H. Stapelfeldt and T. Seideman, Rev. Mod. Phys. **75**, 543 (2003).